A Universal Scheme to Convert Aromatic Molecular Monolayers into Functional Carbon Nanomembranes

Polina Angelova,[†] Henning Vieker,[†] Nils-Eike Weber,[†] Dan Matei,[†] Oliver Reimer,[†] Isabella Meier,[†] Simon Kurasch,[‡] Johannes Biskupek,[‡] Dominik Lorbach,[§] Katrin Wunderlich,[§] Long Chen,[§] Andreas Terfort,[⊥] Markus Klapper,[§] Klaus Müllen,[§] Ute Kaiser,[‡] Armin Gölzhäuser,[†,*] and Andrey Turchanin[†]

[†]Faculty of Physics, University of Bielefeld, 33615 Bielefeld, Germany, [‡]Central Facility of Electron Microscopy, University of Ulm, 89081 Ulm, Germany, [§]Max Planck Institute for Polymer Research, 55128 Mainz, Germany, and [⊥]Institute of Inorganic and Analytical Chemistry, University of Frankfurt, 60438 Frankfurt, Germany

ABSTRACT Free-standing nanomembranes with molecular or atomic thickness are currently explored for separation technologies, electronics, and sensing. Their engineering with well-defined structural and functional properties is a challenge for materials research. Here we present a broadly applicable scheme to create mechanically stable carbon nanomembranes (CNMs) with a thickness of ~0.5 to ~3 nm. Monolayers of polyaromatic molecules (oligophenyls, hexaphenylbenzene, and polycyclic aromatic hydrocarbons) were assembled and exposed to electrons that cross-link them into CNMs; subsequent pyrolysis converts the CNMs into graphene sheets. In this transformation the thickness, porosity, and surface functionality of the nanomembranes are determined by the monolayers, and structural and functional features are passed on from the molecules through their monolayers to the CNMs and finally on to the graphene. Our procedure is scalable to large areas and allows the engineering of ultrathin nanomembranes by controlling the composition and structure of precursor molecules and their monolayers.

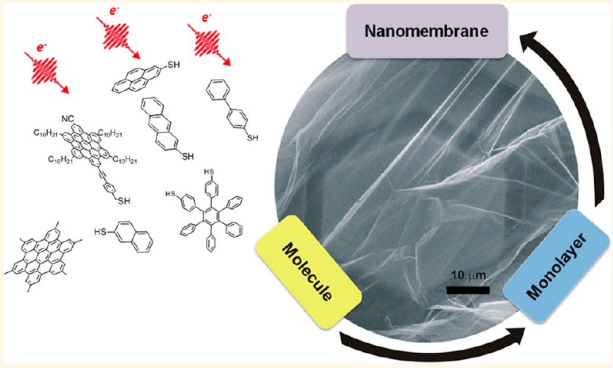

KEYWORDS: two-dimensional materials · carbon nanomembranes · graphene · molecular self-assembly · helium ion microscopy

The creation of functional two-dimensional (2D) materials is a fast-growing field within nanoscience. Nanomembranes,[1] i.e. free-standing films with a thickness of a few nanometers, have been predicted to possess a superior performance in the separation of materials where they should allow a faster passage of the selected—gas or liquid—molecules than any conventional filter.[2] Nanomembranes were integrated in stretchable electronics[3] and have been applied as mechanical resonators in nanoelectro–mechanical systems;[4] further, hybrids of nanomembranes with fluid lipid bilayers were built as biomimetic interfaces for molecular recognition and sensing.[5]

Diverse strategies have been developed to build nanomembranes. Since the 1990s the so-called layer-by-layer (LbL) technique is employed to fabricate membranes for corrosion protection, sensing, and drug delivery.[6,7] In the LbL process, an electrically charged surface is sequentially dipped into positively and negatively charged polyelectrolytes, leading to the formation of polymeric membranes of well-defined molecular composition with thicknesses from ~15 nm to several 100 nm. Much thinner membranes can be made by exfoliating single sheets out of a layered material.[8] Graphene, consisting of a few (~1– 5) layers of carbon atoms, was initially made by exfoliation[9] and is nowadays produced by a variety of techniques,[10] allowing researchers to gain new insights into the physics and chemistry in two dimensions. However, the surface of graphene is homogeneous and chemically inert, which makes an efficient functionalization with other molecules difficult. On the contrary, covalent organic frameworks[11,12] (COFs) and related two-dimensional systems[13–16] are nanomembranes with heterogeneous, chemically reactive surfaces. The first step in

* Address correspondence to ag@uni-bielefeld.de.

Received for review May 26, 2013 and accepted June 26, 2013.

Published online June 26, 2013
10.1021/nn402652f

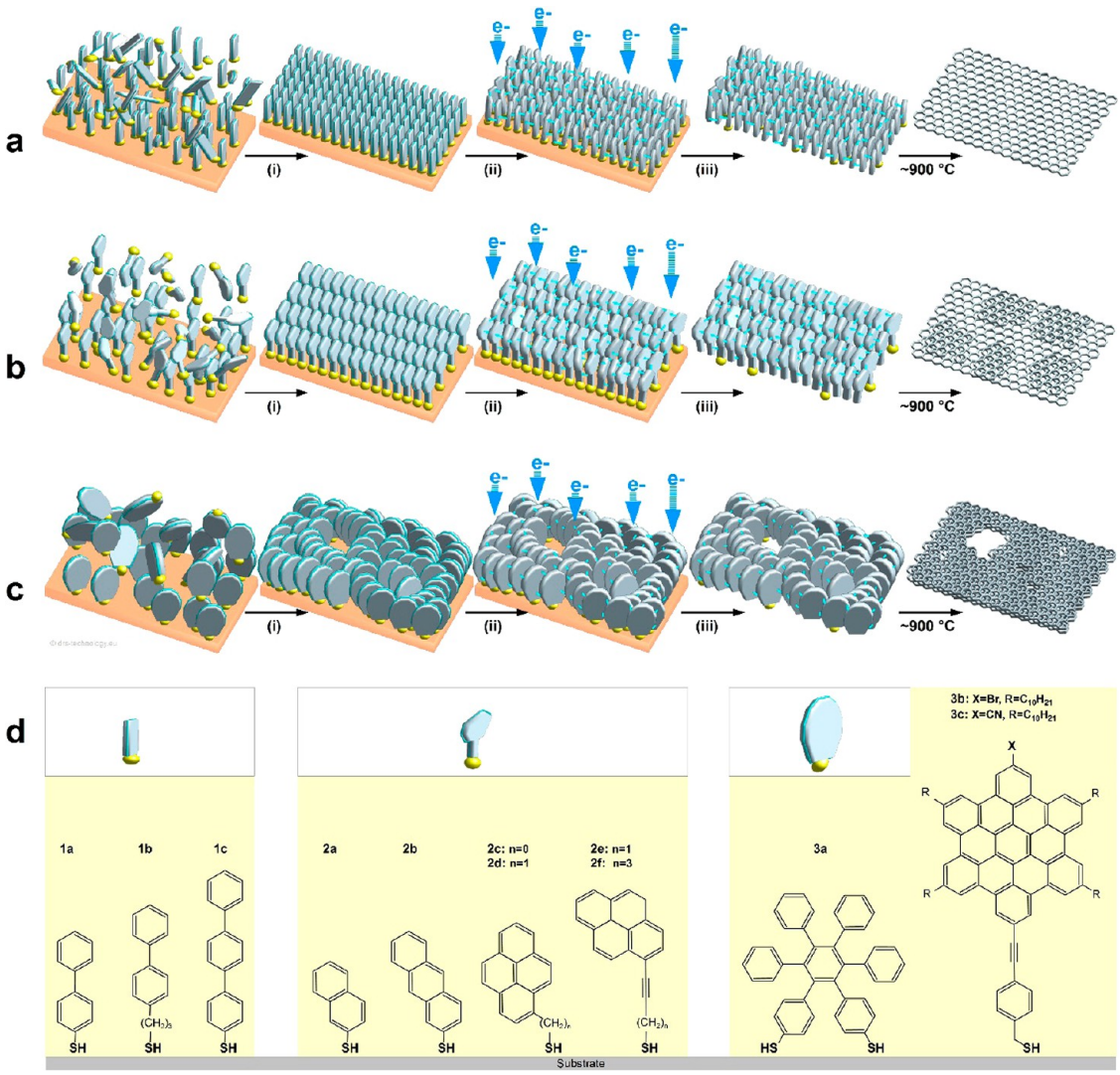

Figure 1. Schematic for the formation of carbon nanomembranes (CNMs) and graphene from molecular precursors. (a–c) Schematic illustration of the fabrication route for CNMs and graphene: Self-assembled monolayers are prepared on a substrate (i), then cross-linked by electron irradiation to form CNMs of monomolecular thickness (ii). The CNMs are released from the underlying substrate (iii), and further annealing at 900 °C transforms them into graphene. (a) Fabrication of thin CNMs and graphene (from "linear" precursor molecules 1a–1c in d). (b) Fabrication of thicker CNMs and few layer graphene sheets (from "condensed" precursors 2a–2f in d). (c) Fabrication of CNMs and graphene sheets with nanopores (from "bulky" precursors 3a–c in d). (d) Chemical structures of the different precursor molecules used in this study.

their creation is the synthesis of organic molecules of well-defined size and shape with functionalities at defined positions. When brought into proximity, adjacent molecules form multiple covalent bonds and assemble, such as Wang tiles, in a 2D lattice. COF nanomembranes look very aesthetic; however, their fabrication is time-consuming and requires high skill in organic synthesis.

In this article, we present a modular and broadly applicable construction scheme to efficiently fabricate ultrathin carbon nanomembranes (CNMs) that unite the thinness of graphene with the chemical functionality of a COF and the ease of fabrication of LbL films. It was found earlier[17] that self-assembled monolayers (SAMs) of 1,1′-biphenyl-4-thiol (BPT) are laterally cross-linked by low-energy electrons and can be removed from the surface forming 1 nm thick CNMs. When these CNMs are pyrolized at ~1000 K, they transform into graphene.[18,19] Motivated by these findings, we applied similar protocols to a variety of other polyaromatic molecules. Our scheme (Figure 1a–c) utilizes a sequence of (i) molecular monolayer assembly on a solid surface, (ii) radiation induced two-dimensional cross-linking, and (iii) a lift-off of the network of cross-linked molecules. The product is a free-standing CNM, whose thickness, homogeneity, presence of pores, and surface chemistry are determined by the nature of the initial molecular monolayer. We investigated three types of thiol-based precursors: nonfused oligophenyl derivatives (Figure 1d: **1a**–**1c**) which possess linear molecular backbones providing an improved structural ordering of the formed SAMs; condensed polycyclic

precursors like naphthalene (NPTH), anthracene (ANTH) and pyrene (MP) mercapto derivatives (Figure 1d: **2a**–**2f**) which are more rigid and should result in a higher stability and an increased carbon density of the monolayers; "bulky" molecules, like the noncondensed hexaphenylbenzene derivative with a propeller-like structure (Figure 1d: **3a**) and extended disc-type polycyclic aromatic hydrocarbons such as hexa-*peri*-benzocoronene (HBC) derivatives (Figure 1d: **3b**,**c**).[20,21] The former are specially functionalized with long alkyl chains and a surface active group which is attached to the π-conjugated backbone through a flexible methylene linker. This molecular design enables a control over the thickness and packing density of the SAMs by varying the conditions of preparation. Figure 1a–c shows schematics of our process applied to different types of monolayers. In Figure 1a oligophenyls with a linear molecular backbone form well-ordered monolayers that cross-link into homogeneous CNMs. After pyrolysis, the CNMs transform into graphene, whose thickness depends on the density of carbon atoms in the monolayers. In Figure 1b, small condensed polycyclic precursors also form monolayers that cross-link into CNMs. After pyrolysis, the CNMs transform into graphene, whose thickness is higher than in **1a**, even if the carbon density is the same as in **1a**. Figure 1c shows bulky aromatic hydrocarbons that assemble in a less-ordered monolayer and cross-link into CNMs with pores. After annealing, these nanomembranes transform into thicker graphene sheets with pores. Hence, the produced graphene takes on structural features from the preceding CNM, which itself has taken on features from the preceding monolayer, i.e. from molecules and surface. Structural and functional properties are thus passed on from the molecules through their monolayers to the nanomembranes. Our procedure is scalable up to square meters and can produce CNMs and graphene of defined thickness, chemical composition and pore density. We investigated how the molecular size, composition, and structure of the monolayers affect the resulting nanomembranes by employing X-ray photoelectron spectroscopy (XPS), scanning tunneling microscopy (STM), low-energy electron diffraction (LEED), helium ion microscopy (HIM), and aberration-corrected high-resolution transmission electron microscopy (HRTEM).

RESULTS AND DISCUSSION

First, we characterized the structure of SAMs on gold from aromatic thiols shown in Figure 1d; Au(111)/mica substrates were immersed into the solutions of the precursor molecules (see Supporting Information (SI) for details of the preparation). SAMs form due to the making of strong bonds between the sulfur and the gold atoms that is accompanied by van der Waals interactions between the carbon atoms.[22] To obtain SAMs with a desired molecular packing, we can adjust parameters like immersion time, temperature, concentration, and polarity of the solvents (see SI). XPS data of aromatic SAMs, representing diverse types of precursors, are shown in Figure 2 (left). For each SAM, its chemical composition and the thickness can be derived from the binding energy and intensity of the C1s, S2p and Au4f photoelectron signals. The sulfur signal consists of a doublet with a $S2p_{3/2}$ binding energy (BE) of 162.0 eV, which unambiguously demonstrates the formation of sulfur–gold bonds.[23] Only for the HBC derivatives (**3b**,**c**), the presence of a second sulfur species with the BE of the $S2p_{3/2}$ signal at 163.6 eV is observed. This signal originates from physisorbed HBC and/or of disulfides,[24] which may be stabilized by π–π interactions between the large aromatic cores, indicating a lower degree of order in these SAMs. Aromatic and aliphatic carbons contribute to the C1s signal at BEs of ~284.2 eV and ~285.0 eV, respectively.[23] Stoichiometry and thickness as obtained from XPS correspond to the composition of the precursor molecules, and indicate the formation of SAMs with an "upright" molecular orientation. By varying the precursors, the thickness of the aromatic monolayers can be adjusted from ~6 Å for NPTH (Figure 1: **2a**) to ~24 Å for HBC–CN (Figure 1: **3c**), which directly correlates with their molecular lengths (see Figure 1a and Table 1). In addition, the temperature and solvent dependent intermolecular interactions of the HBC derivatives[25] allow one to tune the final SAM thickness by varying the preparation conditions (see Table 1). A detailed analysis of the XPS data is presented in Table S1 (see SI).

To determine structure and surface density of the SAMs, they were studied by STM and LEED. Figure 3 shows three molecular precursors containing different numbers of carbon atoms per molecule – anthracene (C14), 3-(biphenyl-4-yl)propane (C15) and terphenyl (C18) thiols. We found that precursor molecules **1b**, **1c**, **2a**, **2b**, **2c**, and **2e** (see Figure 1d) form ordered SAMs with the densely packed[26] ($\sqrt{3} \times \sqrt{3}$) unit cell of the adsorption places and with the ($2\sqrt{3} \times \sqrt{3}$) superstructure of the molecular backbones. These structures are clearly deduced from LEED as well as STM data (see Figure 3) and correspond to a surface area of 21.6 $Å^2$ per molecule. Note that for these SAMs the surface density of carbon atoms in the monolayer can be precisely tuned by the carbon content of the respective molecular precursors. Short biphenylthiols (**1a**) exhibit a (2×2) arrangement of the adsorption places, which corresponds to a less densely packed monolayer of 28.7 $Å^2$ per molecule.[27] We did not observe the formation of LEED patterns and well-ordered SAMs by STM for precursor molecules **2d** and **2f** and **3a**–**c**. As XPS indicates a formation of sulfur–gold bonds for all precursors, we conclude that monolayers of the "bulky" and polycyclic molecules **2d**, **2f**, **3a**–**c** are less ordered and probably less densely packed than the monolayers

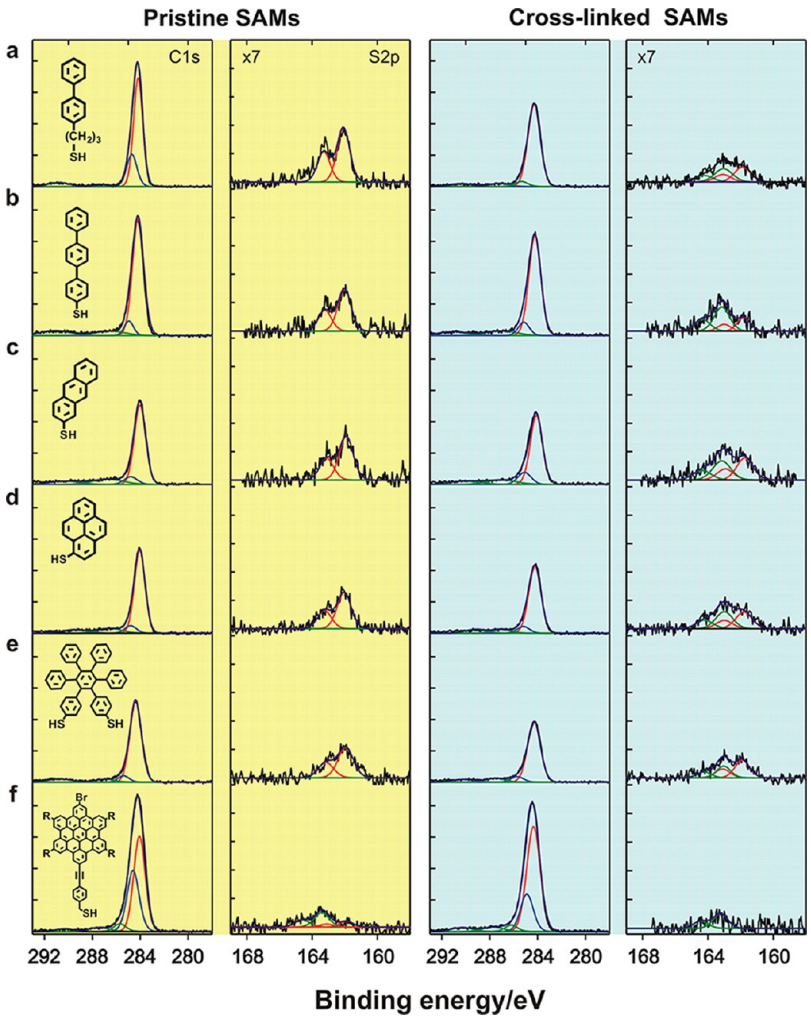

Figure 2. XPS data of pristine SAMs and CNMs. XP spectra of C1s and S2p signals of the pristine (in yellow) and electron-irradiated (50 eV, 60 mC/cm^2) monolayers (in blue) of (a) BP3, 1b. (b) TPT, 1c. (c) ANTH, 2b. (d) 1MP, 2c. (e) HPB, 3a. (f) HBC-Br, 3b.

TABLE 1. Effective thickness of pristine SAMs and CNMs; carbon reduction upon electron irradiation (100 eV, 60 mC/cm^2)

Sample	Thickness SAM [Å]	Thickness CNM [Å]	Reduction of C [%]
1a (BPT)	10	9	5
1b (BP3)	12	10	16
1c (TPT)	13	12	4
2a (NPHT)	6	6	9
2b (ATRH)	9	9	2
2c (1MP)	9	8	10
2d (MP1)	9	8	4
2g (MP3)	11	10	8
2f (MP5)	10	8	11
3a (HPB)	8	8	13
3b^1 (HBC-Br)	10	10	4
3b^2 (HBC-Br)	12	11	5
3b^3 (HBC-Br)	19	17	2
3c^1 (HBC-CN)	12	10	6
3c^2 (HBC-CN)	14	12	5
3c^3 (HBC-CN)	24	22	3

* Different conditions were applied for preparation of SAMs from **3b**$^{1-3}$ and **3c**$^{1-3}$. For details see SI.

of oligophenyls (**1a**−**c**) and the small fused-ring systems (**2a**−**c**, **2e**).

The next step of our process is the radiation-induced conversion of the aromatic monolayers into 2D carbon nanomembranes. Therefore, we irradiated the SAMs with low-energy electrons (50 or 100 eV, see SI), using typical doses of ~60 mC/cm^2, corresponding to ~3500 electrons per 1 nm^2, which leads to a loss of order, as observed in LEED and STM. It is known from previous studies of thiol SAMs[28,29] on gold, that low-energy electron irradiation results in the cleavage of C−H bonds. In aliphatic SAMs, this C−H cleavage is accompanied by conformational changes and C−C cleavage that lead to molecular decomposition and desorption. Conversely, after C−H cleavage in aromatic SAMs, the delocalization of π-electrons over the σ-framework of the aromatic ring, retains its integrity through the irradiation process and we observe a predominant cross-linking between adjacent molecules into a mechanically stable 2D network. As suggested by UV photoelectron spectroscopy and quantum chemical

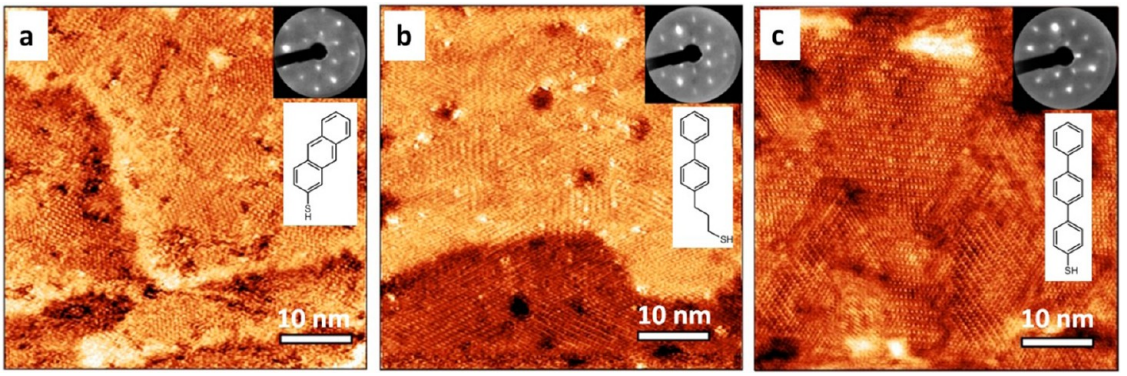

Figure 3. Structure of pristine SAMs. STM micrographs and LEED patterns (insets) of SAMs from molecular precursor: (a) ANTH, 2b; LEED pattern at 116 eV. (b) BP3, 1b; LEED pattern at 127 eV. (c) TPT, 1c; LEED pattern at 129 eV. For molecular structures see Figure 1d.

calculations of BPT SAMs on gold (see Figure 1: **1a**), the formation of single- and double-links (C−C bonds) between phenyl rings of the molecules prevails the cross-linking.[29] Unabling the specificity this picture is also supported by UV−vis spectroscopy of the formed CNMs.[30] Figure 2 shows XPS data before and after electron irradiation in the left and right parts, respectively. As seen from the intensities of the C1s and Au4f (not shown), for purely aromatic SAMs (Figure 2b−d) the irradiation reduces carbon content and monolayer thickness by ∼5−10%; in SAMs with aliphatic chains up to ∼20% (Figure 2a). However, this small loss of material is not relevant for the effectiveness of the cross-linking. We find that the irradiation and the subsequent molecular reorganization also affects the sulfur−gold bonds, as indicated by the appearance of a signal with the $Sp_{3/2}$ binding energy of 163.5 eV, which we assign to thioethers or disulfides forming after the cleavage of S−Au bonds.

After the electron irradiation of the aromatic monolayers, we transferred the obtained CNMs from their gold substrates onto perforated supports (e.g., TEM grids)[18] and imaged them with a helium ion microscope[31] (HIM). This novel charged particle microscopy combines high resolution (∼4 Å) with high surface sensitivity and the possibility to image nonconducting ultrathin specimens.[32] Figure 4 shows HIM micrographs of free-standing CNMs from different types of aromatic molecular precursors (see Figure 1d: **1**−**3**). Simply the fact that one can take these images demonstrates that the SAMs of all these molecules have been cross-linked into mechanically stable CNMs. In Figure 4a−c free-standing CNMs from precursors **1c**, **2c**, and **2d** are shown. These HIM micrographs were acquired at different magnifications, demonstrating the successful fabrication of CNMs of various lateral sizes. The field of view in Figure 4a is 40 × 40 μm^2, which allows to observe some folds in the free-standing 1.2 nm thick CNM. In the lower left corner of Figure 4b, the boundary between the free-standing or supported CNM and substrate can clearly be seen. Figure 4c shows the field of view of 300 × 300 μm^2 with a large and homogeneous CNM of a thickness of 0.8 nm. Macroscopic defects in these nanomembranes are practically negligible on the length scale of these images.

Since the thickness of CNMs is determined by the precursor molecules and their packing density in SAMs, it can be controlled by tailoring these parameters. Figure 4 displays examples of CNMs where the thinnest nanomembrane is from precursor **2a** with a thickness of only 0.6 nm and the thickest one is from precursor **3c** with an about four times higher thickness (2.2 nm). The opportunity to flexibly control the thickness of CNMs opens broad avenues for the engineering of nanomembranes. Along this path, we investigated different CNMs by HIM and found a clear relation between properties of the precursor molecule, its SAMs and the appearance of the ensuing CNM. If the molecule forms a densely packed SAM (**1a**−**c**, **2a**−**c**, **2e** in Figure 1d), the following CNM is continuous and free of holes. Figure 4g shows a high magnification HIM image of a homogeneous CNM made from terphenylthiol (**1c**). Conversely, CNMs made from HBC (**3b**−**c** in Figure 1d) or HPB (**3a** in Figure 1d) precursors, two molecules that possess larger sizes and form less well-ordered SAMs, exhibit pores, cf. the HIM images in Figure 4h and Figure 4i. The dark spots in these images are pores that have a very small diameter and a narrow size distribution, as shown in the respective histograms (see insets). In case of the HBC precursor the mean size of the nanopores is ∼6 nm with the surface density of 9.1 × 10^{14} pores/m^2; the more compact HPB precursor shows a size of ∼2.4 nm with a surface density of 1.3 × 10^{15} pores/m^2. The formation of nanopores in these CNMs is thus attributed to the large van der Waals radii of HBC and HPB structures and in the case of HBCs to the propensity of the disk like molecules for intermolecular stacking which competes with the molecule−substrate interactions and lowers the order in the respective SAMs. We also observe that the average pore diameter decreases from 6.4 to 3.0 nm

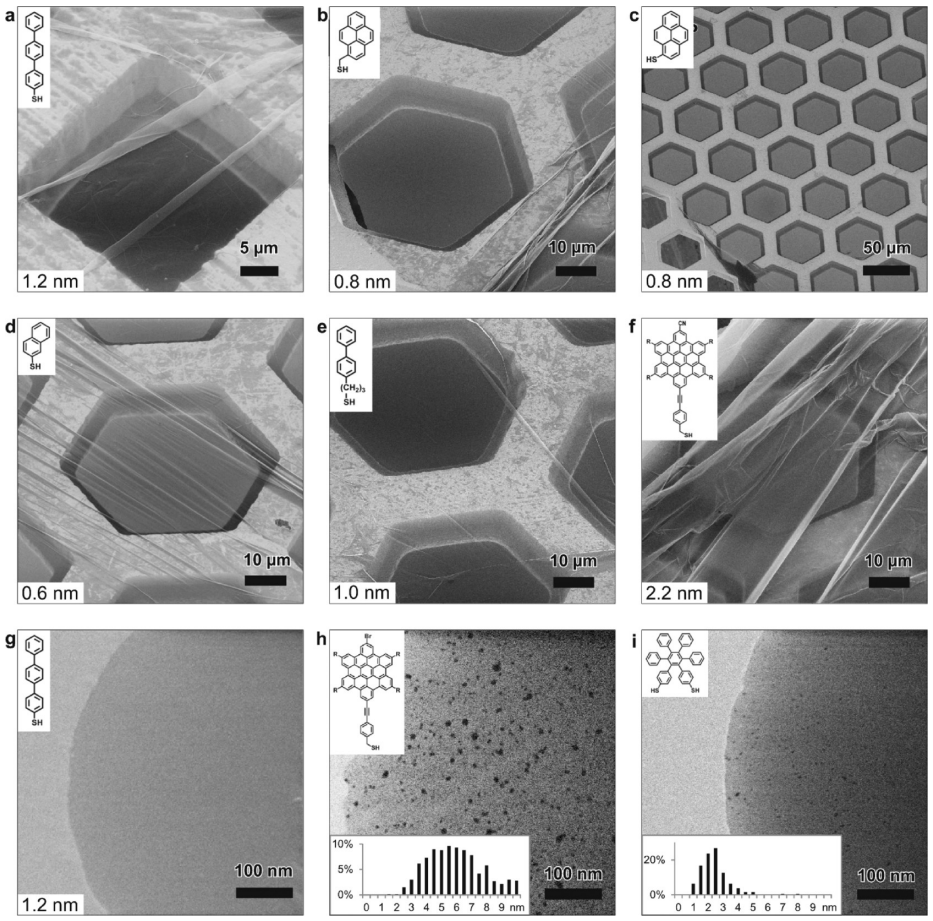

Figure 4. Helium ion microscope (HIM) micrographs of free-standing CNMs. After cross-linking the nanomembranes were transferred onto TEM grids and images were taken at different magnifications (see scale bar). CNMs were prepared from: (a) TPT, 1c; (b) MP1, 2d; (c) 1MP, 2c; (d) NPTH, 2a; (e) BP3, 2b; (f) HBC−CN, 3c; (g) TPT, 1c; (h) HBC-Br, 3b; (i) HPB, 3a; the upper left insets show the precursor molecules. The CNM in a is suspended over a gold TEM grid, CNMs in (b−f) over copper grids, CNMs in (g−i) over Cu grids with thin carbon film. The numbers in the lower left corners in (a−g) indicate the CNM thicknesses, as determined from XPS before the transfer. HIM images (h and i) show CNMs with nanopores, the lower insets show the respective distributions (in %) of pore diameters (in nm).

when the SAM thickness increases from 1 to 2 nm (see SI for details).

Finally, we studied the conversion of CNMs from various molecular precursors into graphene[19] by annealing them at 900 °C in ultrahigh vacuum (~10^{-9} mbar) (see SI for details). Sulfur atoms, initially present in the CNM (see Figure 1d), desorb during this treatment.[29] Note that a high thermal stability of CNMs is essential for the conversion into graphene, as non-electron-irradiated aromatic thiol SAMs desorb from the substrate at temperatures[33] (~120 °C) that are much lower than necessary for their pyrolysis. The atomic structure of the CNMs after annealing was imaged by aberration-corrected (AC) high-resolution transmission electron microscopy (HRTEM) at 80 kV accelerating voltage. The atomically resolved AC-HRTEM micrographs of annealed CNMs from various precursor molecules are presented in Figure 5; in these images carbon atoms appear dark. Figure 5a shows one of the thinnest CNMs (0.8 nm, **3a** in Figure 1d) after annealing. Most of the sheet area consists of single-layer graphene (~50%, light-blue color coded) with the clearly recognizable hexagonal arrangement of carbon atoms; randomly oriented graphene nanocrystallites are connected with each other *via* the typical heptagon−pentagon[34] grain boundaries (see inset to Figure 5a). A small fraction of the sheet (~20%, light green color coded) consists of graphene double-layers, which reveals the respective moiré pattern.[35] Gray and light-red areas correspond to the disordered carbon and holes, respectively; pentagons (green) and heptagons (blue) are marked. The thickness of the formed graphene sheets depends on the structure of the precursor molecules and their abilities to form SAMs and to be cross-linked into CNMs. As seen in Figure 5b−g, graphene sheets from various precursors have the same nanocrystalline morphology as in Figure 5a; however, their thickness varies by a factor of ~3, depending on the precursor. This visual impression was confirmed by measuring the film thickness by quantitative electron energy loss spectroscopy (EELS) at the carbon K adsorption edge[36] (see SI, Table S2). The structural transformation of CNMs into

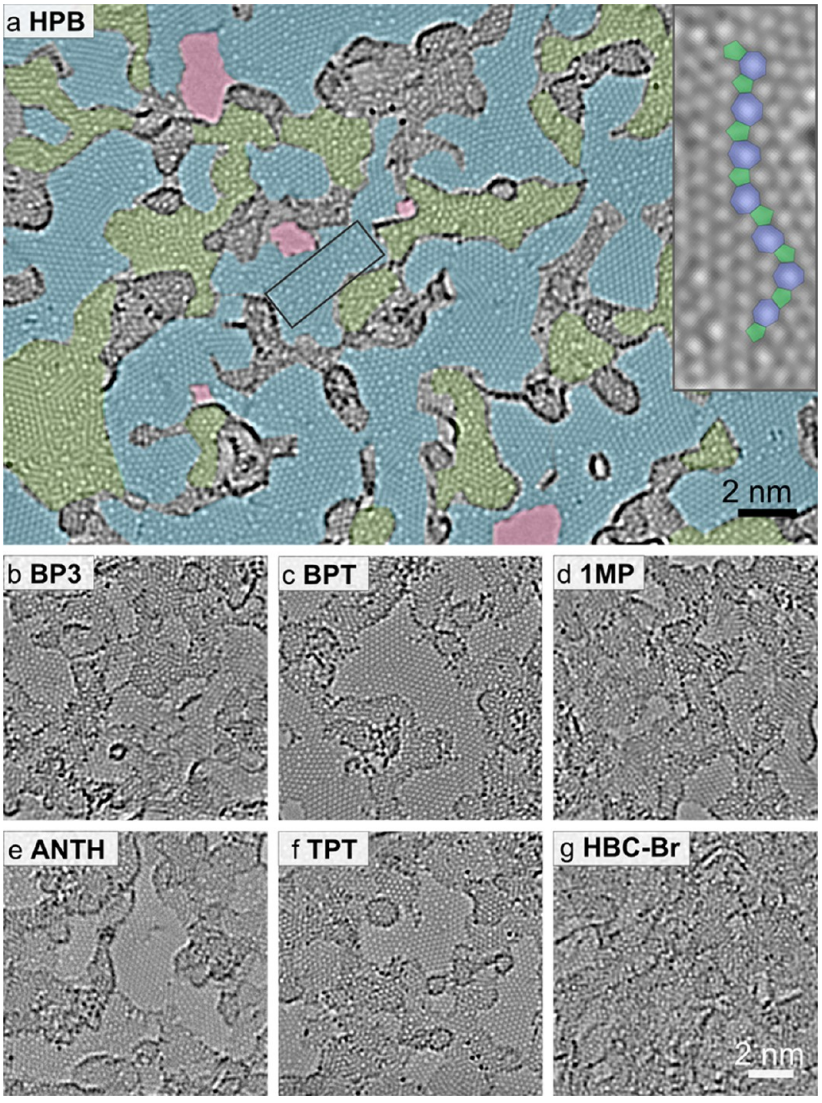

Figure 5. Atomic structure of CNMs of various thicknesses after conversion into graphene. Aberration-corrected high-resolution transmission electron microscope (AC-HRTEM) images at 80 kV of graphene samples, prepared from (a) HPB, 3a. (b) biphenylthiol, BP3, 1b. (c) BPT, 1a. (d) 1MP, 2c. (e) ANTH, 2b. (f) TPT, 1c. (g) HBC-Br, 3b. Regions of different layer thicknesses are color coded: single layers - light blue; double layers - light green; holes - light red. The insert in (a) shows a magnified grain boundary where arrangements of carbon atoms into pentagons (green) and heptagons (blue) are marked. For structures of the molecular precursors see Figure 1d.

graphene has a drastic impact on the electrical properties. Being initially dielectric, with a band gap of ~4 eV for CNMs from biphenylthiols[29] (**1a** in Figure 1d), annealing at 900 °C results in the conversion into conductive graphene with a sheet resistivity of ~100–500 kΩ/sq. The resistivity correlates with the thickness of the graphene sheets, with lower resistivity for the thicker sheets.

The above results clearly demonstrate that our procedure is a modular and broadly applicable construction scheme to fabricate nanomembranes that adopt properties from their preceding molecular monolayers. As the process utilizes electron-beam exposures, the size of the irradiated area can be varied. With a flooded (defocused) exposure, large area (up to m^2) CNM and graphene sheets can be fabricated. With a focused electron beam lithography exposure, micro- and nanometer sized sheets can be written.[37] In this study only thiols on gold were investigated; however, the fabrication of nanomembrane and graphene sheets can be expanded to a variety of other metal surfaces using sulfur-, nitrogen-, or phosphorus-containing surface active compounds as well as onto insulator and semiconductor substrates using hydroxy-[38] or silane-derivatives.[17] This flexibility allows a direct growth of CNM or graphene on technologically relevant substrates.

In order to become nanomembranes, the SAMs first need a stable scaffold that is rigid enough to sustain the electron irradiation and that can form intermolecular cross-links. Second, they have to possess a sufficient density of carbon atoms. These conditions are fulfilled by SAMs with a fair amount of aromatic

groups. While SAMs from all molecules in Figure 1d can be converted into nanomembranes, monoaryl or short molecules such as pyridine-4-thiol and anthracene-9-thiol cannot. The shortest precursor that led to CNMs and graphene sheets was naphthalene-2-thiol (Figure 1d: **2a**) consisting of two fused benzene rings. Remarkably enough, the thickness of the formed sheets correlates with the density of carbon in the SAMs and with the packing of the constituting molecules. By selecting appropriate precursor molecules, large areas of single-layer graphene can thus be produced. Polycyclic aromatic hydrocarbons (Figure 1d: **2a**–**f**) led to thicker CNM and graphene sheets than oligophenyls with the same surface density of carbon atoms (Figure 1d: **1a**–**d**). Pristine SAMs of high structural quality result in the homogeneous CNM and homogeneous graphene sheets (see Figure 4g), whereas SAMs of low structural quality result in sheets with nanopores (Figure 4h, Figure 4i). The size of the resulting nanopores is quite small and varies from ~1 to 10 nm (see SI), as it mainly depends on the precursor molecules and their packing density in the SAMs; one may tailor the CNMs for applications in ultrafiltration.[39] Some CNMs can form Janus nanomembranes[40] with two distinct faces possessing amino- and thiol-groups, respectively, allowing selective chemical functionalization on both faces. A chemical functionalization of CNMs, together with opportunities to mix precursor molecules, opens many doors to engineer novel 2D hybrid materials.

CONCLUSIONS

We have presented a universal and scalable route to ultrathin free-standing carbon nanomembranes and graphene using aromatic molecules as precursors. The properties of the resulting sheets can be flexibly adjusted including their thickness, conductivity, chemical functionalization, and appearance of nanopores. We expect that, due to its simplicity and universality, the approach will have a strong impact on (1) the rapidly growing field of free-standing 2D materials and facilitate their incorporation and application in NEMS devices and (2) the separation of molecules as metal-free catalysts or when properly functionalized as bio- or chemically sensing coatings.

EXPERIMENTAL METHODS

Samples Preparation. Molecular precursors used in this study are commercially available (**1a** and **2a**) or were specially synthesized (**1b**–**c**, **2b**–**f**, **3a**–**c**). SAMs were prepared by immersion of 300 nm thermally evaporated Au on mica substrates into the respective solvents (see SI for details). Cross-linking was achieved either in an ultrahigh vacuum (UHV) ($<10^{-9}$ mbar) chamber or in a high vacuum (HV) ($<5 \times 10^{-7}$ mbar) chamber employing 50 and 100 eV electrons, respectively, and a dose of ~60 mC/cm^2. All XPS, LEED, and STM measurements were conducted on samples cross-linked *in situ* in the UHV chamber of XPS. For HIM and TEM measurements both samples cross-linked in the UHV chamber and in the HV chamber were employed. Transfer of CNMs and graphene onto TEM grid was conducted by spin-coating on their surface 500-nm-thick layers of poly(methyl methacrylate) (PMMA), etching the original gold substrates, transferring the CNM/PMMA or graphene/PMMA sandwiches onto TEM grids, and dissolving PMMA in acetone using a critical point dryer.[18] Annealing of the samples mounted in molybdenum sample holders was conducted for 30 min at 900 °C in an UHV chamber (5×10^{-9} mbar) using heating/cooling rates of 400 °C/h.

Characterization. The as-prepared SAMs and CNMs were analyzed by XPS, STM, and LEED in a multichamber UHV-system (Omicron). STM images were obtained using electrochemically etched tungsten tips, with tunneling currents of 30–50 pA and bias voltages of 300 mV. LEED patterns were recorded using a BDL600IR-MCP instrument (OCI Vacuum Microengineering) with a multichannel plate (MCP) detector with the electron beam currents below 1 nA. XPS was performed using a monochromatic X-ray source (Al Kα) and a Sphera electron analyzer (Omicron) with a resolution of 0.9 eV. HIM was conducted with a Carl Zeiss Orion Plus. The He^+ ion beam was operated at 33–37 kV acceleration voltage at currents of 0.2–0.4 pA. A working distance of 8–22 mm was employed, and secondary electrons were collected by an Everhart-Thornley detector. AC-HRTEM characterization was conducted with an aberration-corrected FEI Titan microscope operated at a beam energy of 80 kV to minimize knock-on damage and equipped with a postcolumn Gatan energy filter for local EELS analysis. Electrical measurements were done by a standard four-point setup using Suess probes and a Keithley source-measure unit.

Full Methods are available in the Supporting Information.

Conflict of Interest: The authors declare no competing financial interest.

Acknowledgment. This work was supported by the German Bundesministerium für Bildung und Forschung (BMBF, Grants 03X0108A and 03X0108B) and by the Deutsche Forschungsgemeinschaft (DFG) through priority program SPP1459 "Graphene" (Grants TU149/2-1 and KA1295/15-1). A.Tu. further thanks the DFG for a Heisenberg Fellowship (TU149/3-1). S.K., J.B. and U.K. thank the state Baden-Württemberg for financial support within SALVE (KA 1295/17-2).

Supporting Information Available: Description of materials, full description of methods, interpretation of XPS spectra, summary of EELS data, evaluation of porosity of HBC-based nanomembranes, and supporting references. This material is available free of charge via the Internet at http://pubs.acs.org.

REFERENCES AND NOTES

1. Rogers, J. A.; Lagally, M. G.; Nuzzo, R. G. Synthesis, Assembly and Applications of Semiconductor Nanomembranes. *Nature* **2011**, *477*, 45–53.
2. Wang, E. N.; Karnik, R. Water Desalination: Graphene Cleans up Water. *Nat. Nanotechnol.* **2012**, *7*, 552–554.
3. Li, X. S.; Cai, W. W.; An, J. H.; Kim, S.; Nah, J.; Yang, D. X.; Piner, R.; Velamakanni, A.; Jung, I.; Tutuc, E.; et al. Large-Area Synthesis of High-Quality and Uniform Graphene Films on Copper Foils. *Science* **2009**, *324*, 1312–1314.
4. Zande, A. M. v. d.; Barton, R. A.; Alden, J. S.; Ruiz-Vargas, C. S.; Whitney, W. S.; Pham, P. H. Q.; Park, J.; Parpia, J. M.; Craighead, H. G.; McEuen, P. L. Large-Scale Arrays of Single-Layer Graphene Resonators. *Nano Lett.* **2010**, *10*, 4869–4873.
5. Ang, P. K.; Jaiswal, M.; Lim, C. H. Y. X.; Wang, Y.; Sankaran, J.; Li, A.; Lim, C. T.; Wohland, T.; Barbaros, Ö.; Loh, K. P. A Bioelectronic Platform Using a Graphene–Lipid Bilayer Interface. *ACS Nano* **2010**, *4*, 7387–7394.
6. Lvov, Y.; Decher, G.; Möhwald, H. Assembly, Structural Characterization, and Thermal Behavior of Layer-by-Layer

Deposited Ultrathin Films of Poly(vinylsulfate) and Poly(allylamine). *Langmuir* **1993**, *9*, 481–486.
7. Decher, G. Fuzzy Nanoassemblies: Toward Layered Polymeric Multicomposites. *Science* **1997**, *277*, 1232–1237.
8. Novoselov, K. S.; Jiang, D.; Schedin, F.; Booth, T. J.; Khotkevich, V. V.; Morozov, S. V.; Geim, A. K. Two-Dimensional Atomic Crystals. *Proc. Natl. Acad. Sci. U.S.A.* **2005**, *102*, 10451–10453.
9. Geim, A. K.; Novoselov, K. S. The Rise of Graphene. *Nat. Mater.* **2007**, *6*, 183–191.
10. Novoselov, K. S.; Fal'ko, V. I.; Colombo, L.; Gellert, P. R.; Schwab, M. G.; Kim, K. A Roadmap for Graphene. *Nature* **2012**, *490*, 192–200.
11. Cote, A. P.; Benin, A. I.; Ockwig, N. W.; O'Keeffe, M.; Matzger, A. J.; Yaghi, O. M. Porous, Crystalline, Covalent Organic Frameworks. *Science* **2005**, *310*, 1166–1170.
12. Colson, J. W.; Woll, A. R.; Mukherjee, A.; Levendorf, M. P.; Spitler, E. L.; Shields, V. B.; Spencer, M. G.; Park, J.; Dichtel, W. R. Oriented 2D Covalent Organic Framework Thin Films on Single-Layer Graphene. *Science* **2011**, *332*, 228–231.
13. Grill, L.; Dyer, M.; Lafferentz, L.; Persson, M.; Peters, M. V.; Hecht, S. Nano-Architectures by Covalent Assembly of Molecular Building Blocks. *Nat. Nanotechnol.* **2007**, *2*, 687–691.
14. Kissel, P.; Erni, R.; Schweizer, W. B.; Rossell, M. D.; King, B. T.; Bauer, T.; Gotzinger, S.; Schluter, A. D.; Sakamoto, J. A Two-Dimensional Polymer Prepared by Organic Synthesis. *Nat. Chem.* **2012**, *4*, 287–291.
15. Schultz, M. J.; Zhang, X. Y.; Unarunotai, S.; Khang, D. Y.; Cao, Q.; Wang, C. J.; Lei, C. H.; MacLaren, S.; Soares, J.; Petrov, I.; et al. Synthesis of Linked Carbon Monolayers: Films, Balloons, Tubes, and Pleated Sheets. *Proc. Natl. Acad. Sci. U.S.A.* **2008**, *105*, 7353–7358.
16. Bauer, T.; Zheng, Z. K.; Renn, A.; Enning, R.; Stemmer, A.; Sakamoto, J.; Schlüter, A. D. Synthesis of Free-Standing, Monolayered Organometallic Sheets at the Air/Water Interface. *Angew. Chem., Int. Ed.* **2011**, *50*, 7879–7884.
17. Eck, W.; Küller, A.; Grunze, M.; Völkel, B.; Gölzhäuser, A. Freestanding Nanosheets from Crosslinked Biphenyl Self-Assembled Monolayers. *Adv. Mater.* **2005**, *17*, 2583–2587.
18. Turchanin, A.; Beyer, A.; Nottbohm, C. T.; Zhang, X.; Stosch, R.; Sologubenko, A. S.; Mayer, J.; Hinze, P.; Weimann, T.; Gölzhäuser, A. One Nanometer Thin Carbon Nanosheets with Tunable Conductivity and Stiffness. *Adv. Mater.* **2009**, *21*, 1233–1237.
19. Turchanin, A.; Weber, D.; Büenfeld, M.; Kisielowski, C.; Fistul, M. V.; Efetov, K. B.; Weimann, T.; Stosch, R.; Mayer, J.; Gölzhäuser, A. Conversion of Self-Assembled Monolayers into Nanocrystalline Graphene: Structure and Electric Transport. *ACS Nano* **2011**, *5*, 3896–3904.
20. Feng, X.; Pisula, W.; Zhi, L.; Takase, M.; Müllen, K. Controlling the Columnar Orientation of C3-Symmetric "Superbenzenes" through Alternating Polar/Apolar Substitutents. *Angew. Chem., Int. Ed.* **2008**, *47*, 1703–1706.
21. Wagner, C.; Kasemann, D.; Golnik, C.; Forker, R.; Esslinger, M.; Müllen, K.; Fritz, T. Repulsion between Molecules on a Metal: Monolayers and Submonolayers of Hexa-peri-hexabenzocoronene on Au(111). *Phys. Rev. B* **2010**, *81*, 035423.
22. Love, J. C.; Estroff, L. A.; Kriebel, J. K.; Nuzzo, R. G.; Whitesides, G. M. Self-Assembled Monolayers of Thiolates on Metals as a Form of Nanotechnology. *Chem. Rev.* **2005**, *105*, 1103–1169.
23. Zharnikov, M.; Grunze, M. Spectroscopic Characterization of Thiol-Derived Self-Assembling Monolayers. *J. Phys.: Condens. Matter* **2001**, *13*, 11333–11365.
24. Castner, D. G.; Hinds, K.; Grainger, D. W. X-ray Photoelectron Spectroscopy Sulfur 2p Study of Organic Thiol and Disulfide Binding Interactions with Gold Surfaces. *Langmuir* **1996**, *12*, 5083–5086.
25. Kastler, M.; Pisula, W.; Wasserfallen, D.; Pakula, T.; Müllen, K. Influence of Alkyl Substituents on the Solution- and Surface-Organization of Hexa-Peri-Hexabenzocoronenes. *J. Am. Chem. Soc.* **2005**, *127*, 4286–4296.
26. Vericat, C.; Vela, M. E.; Benitez, G.; Carro, P.; Salvarezza, R. C. Self-Assembled Monolayers of Thiols and Dithiols on Gold: New Challenges for a Well-Known System. *Chem. Soc. Rev.* **2010**, *39*, 1805–1834.
27. Matei, D. G.; Muzik, H.; Gölzhäuser, A.; Turchanin, A. Structural Investigation of 1,1′-Biphenyl-4-thiol Self-Assembled Monolayers on Au(111) by Scanning Tunneling Microscopy and Low-Energy Electron Diffraction. *Langmuir* **2012**, *28*, 13905–13911.
28. Zharnikov, M.; Frey, S.; Heister, K.; Grunze, M. Modification of Alkanethiolate Monolayers by Low Energy Electron Irradiation: Dependence on the Substrate Material and on the Length and Isotopic Composition of the Alkyl Chains. *Langmuir* **2000**, *16*, 2697–2705.
29. Turchanin, A.; Käfer, D.; El-Desawy, M.; Wöll, C.; Witte, G.; Gölzhäuser, A. Molecular Mechanisms of Electron-Induced Cross-Linking in Aromatic SAMs. *Langmuir* **2009**, *25*, 7342–7352.
30. Nottbohm, C. T.; Turchanin, A.; Beyer, A.; Stosch, R.; Gölzhäuser, A. Mechanically Stacked 1-nm-thick Carbon Nanosheets: Ultrathin Layered Materials with Tunable Optical, Chemical, and Electrical Properties. *Small* **2011**, *7*, 874–883.
31. Ward, B. W.; Notte, J. A.; Economou, N. P. Helium Ion Microscope: A New Tool for Nanoscale Microscopy and Metrology. *J. Vac. Sci. Technol., B* **2006**, *24*, 2871–2874.
32. Bell, D. C. Contrast Mechanisms and Image Formation in Helium Ion Microscopy. *Microsc. Microanal.* **2009**, *15*, 147–153.
33. Turchanin, A.; El-Desawy, M.; Gölzhäuser, A. High Thermal Stability of Cross-Linked Aromatic Self-Assembled Monolayers: Nanopatterning *via* Selective Thermal Desorption. *Appl. Phys. Lett.* **2007**, *90*, 053102.
34. Kim, K.; Lee, Z.; Regan, W.; Kisielowski, C.; Crommie, M. F.; Zettl, A. Grain Boundary Mapping in Polycrystalline Graphene. *ACS Nano* **2011**, *5*, 2142–2146.
35. Warner, J. H.; Rummeli, M. H.; Gemming, T.; Buchner, B.; Briggs, G. A. D. Direct Imaging of Rotational Stacking Faults in Few Layer Graphene. *Nano Lett.* **2009**, *9*, 102–106.
36. Egerton, R. F.; Malac, M. Improved Background-Fitting Algorithms for Ionization Edges in Electron Energy-Loss Spectra. *Ultramicroscopy* **2002**, *92*, 47–56.
37. Nottbohm, C. T.; Turchanin, A.; Beyer, A.; Golzhauser, A. Direct e-Beam Writing of 1 nm Thin Carbon Nanoribbons. *J. Vac. Sci. Technol., B* **2009**, *27*, 3059–3062.
38. Küller, A.; Eck, W.; Stadler, V.; Geyer, W.; Gölzhäuser, A. Nanostructuring of Silicon by Electron-Beam Lithography of Self-Assembled Hydroxybiphenyl Monolayers. *Appl. Phys. Lett.* **2003**, *82*, 3776–3778.
39. Striemer, C. C.; Gaborski, T. R.; McGrath, J. L.; Fauchet, P. M. Charge- and Size-Based Separation of Macromolecules Using Ultrathin Silicon Membranes. *Nature* **2007**, *445*, 749–753.
40. Zheng, Z.; Nottbohm, C. T.; Turchanin, A.; Muzik, H.; Beyer, A.; Heilemann, M.; Sauer, M.; Gölzhäuser, A. Janus Nanomembranes: A Generic Platform for Chemistry in Two Dimensions. *Angew. Chem., Int. Ed.* **2010**, *49*, 8493–8497.